Available online at https://link.springer.com/journal/42241
http://www.jhydrodynamics.com
Journal of Hydrodynamics, 2022, 34(6): 1067-1080
https://doi.org/10.1007/s42241-022-0083-7

Near-bed hydrodynamics associated with the entrainment of coarse particles at different protrusion heights

Yushu Xie[1], Bruce W. Melville[1], Asaad Y. Shamseldin[1], Colin N. Whittaker[1], Yifan Yang[2*]
1. *Department of Civil and Environmental Engineering, The University of Auckland, Auckland, New Zealand*
2. *School of Engineering, The University of Waikato, Hamilton, New Zealand*

(Received April 19, 2022, Revised July 13, 2022, Accepted July 19, 2022, Published online December 14, 2022)

Abstract: This paper presents an investigation of near-bed hydrodynamics for a protruding coarse particle over a regular roughened bed. The laboratory experiments were undertaken at the threshold flow condition, which induced dislodgement of the protruding particle. Using different protrusion heights, the experimental results show that the protruding particle substantially changed the spatial distributions of time-averaged velocities, turbulent kinetic energy, and Reynolds shear stress when compared with those obtained from a flat rough bed. The spatial distribution pattern of the flow characteristics shows a reasonable degree of similarity at different protrusion heights examined in this study. Above the target particle, a zone of low Reynolds shear stress was observed. Quadrant analysis was conducted along the main flow direction, at an elevation close to the top of the target particle. A prevalence of sweep (Quadrant 4) and outwards interaction (Quadrant 1) events were associated with the dislodgement of the protruding particle. These findings imply that the drag force related to strong streamwise velocities may play a more significant role in protruding particle entrainment than the shear stress.

Key words: Entrainment, particle protrusion, flow structure, shear stress, quadrant analysis

Introduction

In natural streams, the complex bed morphology is often composed of discrete protruding particles. The particle protrusion induces a separation zone and large-scale flow structures in its vicinity. The variations of the flow structure potentially affect the transportation of underlying sediment particles. Thus, various studies have been done to investigate the hydrodynamics near a protruding particle, including Yager et al.[1], Grams and Wilcock[2] and Raus et al. [3] etc. The presence of the protruding particle increases the shear stress, but it is not entirely responsible for the bed sediment motion. Grams and Wilcock[2] observed that the transportation rate of the bed sediment is dependent on the protrusion height. As the protrusion height increases, the entrainment rate first increases and then decreases with further increases in protrusion height. They concluded that a particle with a high relative protrusion provides a shelter region for the adjacent sediment particles, which causes a decrease in the entrainment rate. In these studies, the protruded particle is considered immobile, and more attention was focused on the transportation of underlying finer particles. However, Wiberg and Smith[4] found that the highly protruding particle is prone to dislodgement since a large proportion of the particle's cross-sectional area is exposed to the turbulent flow, even for a poorly sorted sediment bed. Additionally, the dislodgement of a single coarse particle directly exposes the underlying sediment particles to the shear flow, which can further affect the transport rate. Hence, the dislodgement threshold flow condition of a single protruding coarse particle is fundamentally important.

The influence of protrusion on the initial particle movement was recognised by Fenton and Abbott[5], who systematically studied the protrusion effect on the dislodgement threshold flow condition of an individual particle. Later, this idea was further investigated by Vollmer and Kleinhans[6] through analytical methods and by Chin[7], Coleman et al.[8] in laboratory experiments. These studies mainly considered particle protrusion as a critical factor to explain the data scatter in the theoretical Shields diagram. However, the distribution of the flow characteristics near the particle has received less attention. Cameron[9], Dwivedi et al.[10] presented experimental results about

Biography: Yushu Xie (1992-), Female, Ph. D.,
E-mail: yxie399@aucklanduni.ac.nz
Corresponding author: Yifan Yang,
E-mail: yifan.yang@waikato.ac.nz

the hydrodynamics near a protruding particle at the threshold flow condition. In their experiments, the relative particle protrusion height P/d was relatively low (i.e., $P/d < 0.25$, where P is the protrusion height over the top of the roughness bed, d is the diameter of the protruded particle). According to the finding reported by Raus et al.[3], the near-bed flow regimes exhibited distinguishable behaviour above and below $P/d = 0.40$. Within the medium to high protrusion range $(P/d > 0.40)$, the correlation between the affected flow characteristics and the entrainment of the protruding particle requires more investigation.

The flow characteristics can provide fundamental information for estimating the threshold condition. Additionally, the role of turbulence cannot be neglected. According to quadrant analysis, the component of streamwise velocity u' and vertical velocity component v' can be classified into four types of turbulent events: outward interactions in the first quadrant ($u'>0$, $v'>0$), ejections in the second quadrant ($u'<0$, $v'>0$), inward interactions in the third quadrant ($u'<0$, $v'<0$), and sweeps in the fourth quadrant ($u'>0$, $v'>0$). Sweep, and ejection events were widely accepted as responsible for particle dislodgement since they contribute positively to the Reynolds shear stress[9-13]. However, Thorne et al.[14], Nelson et al.[15] and Cecchetto et al.[16] observed that the outward interaction is responsible for particle entrainment. The different conclusions indicate that a thorough understanding of the impact of turbulent bursts on particle entrainment remains elusive. One possible reason for such a variation might be the choice in previous studies of a single location for quadrant analysis. For example, Cecchetto et al.[16], Wu and Shih[17] observed outward interaction events at a location very close to the target particle, whereas Cameron[9], Dwivedi et al.[10] reported sweep events at $0.5d$ upstream the target particle. This factor is important when it comes to analysing the entrainment of a highly protruded particle, where the turbulent events around the particle have many variations[18].

The main objective of the current study is to conduct an experimental investigation of the flow characteristics near a high protruding particle $(P/d > 0.50)$ under the threshold flow condition associated with the entrainment of the protruded particle. The turbulent events around the particle are presented and their influence on the particle entrainment is discussed.

1. Experimental setup and methods

Experiments were carried out in a 12.00 m long, 0.44 m wide recirculating flume, which has glass sidewalls facilitating visual observation and video recording. The water in the flume is recirculated by a water pump controlled electronically. A set of mesh grids is installed at the upstream inlet of the channel to suppress water surface undulations. A 4.5 m long roughness layer (i.e., the test section) is set up in the channel at 4.0 m downstream of the flow inlet to simulate the conceptualised natural bed roughness. In the roughened section, hemispheres with uniform diameters are installed with a compact hexagonal-packing pattern. A 1.2 m long reach made of 20 mm-30 mm natural gravels was installed upstream and downstream of the roughened section to smoothen flow transition. The schematic display of the experimental flume was presented in Fig. 1.

A spherical particle is used in the present study to investigate the entrainment process of coarse grains over a rough bed. The term "target particle" is used to represent this particle hereinafter to avoid ambiguity. The target particle is made of carbon material, with a diameter of $d = 30$ mm and a mass of 0.016 kg, resulting in a density of 1 137 kg/m^3. In this study, the particle protrusion height P is defined as the distance between the top of the target particle and the upper surface of the bed roughness spheres, as shown in Fig. 2. At the upstream face of the target particle, a customised 3D-printed device (i.e., the grey object in Fig. 2) was used to support the target particle. This support device comprised a hemisphere mounted on a cylinder with a diameter of $D = 40$ mm, which is the

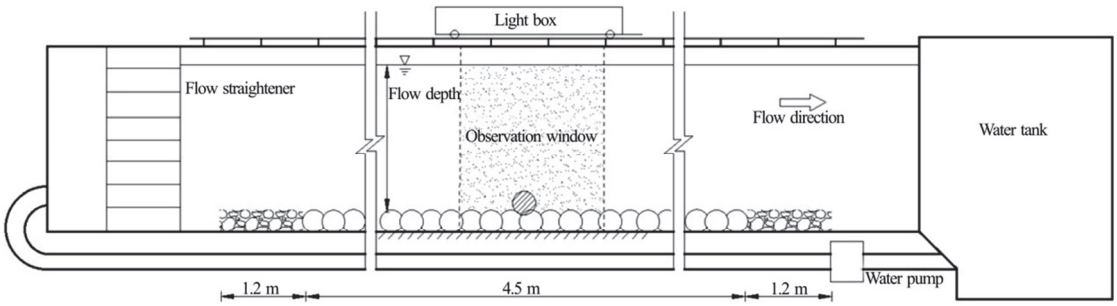

Fig. 1 Schematic drawing of the experimental set-up in the flume

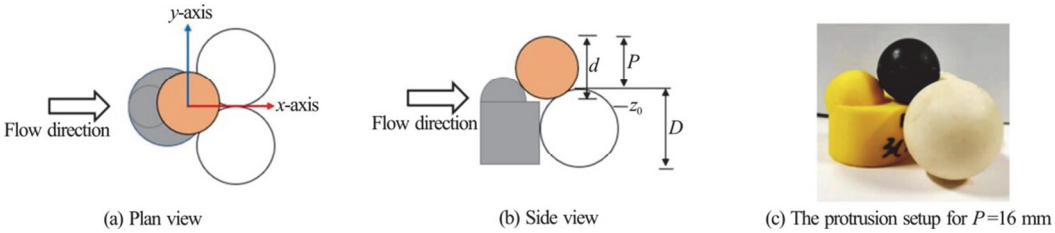

(a) Plan view (b) Side view (c) The protrusion setup for P=16 mm

Fig. 2 (Color online) The schematic diagram of particle setup. The orange circle, blank circle and grey shape indicate the target particle, bed roughness, and support device

same as the diameter of other surrounding bed roughness elements. The size of the mounted hemisphere is adjusted to create four different protrusion heights of the target particle, i.e., $P = 16.0$ mm, 18.0 mm, 20.0 mm and 21.3 mm. Here, the relative protrusion is defined as the ratio of the protrusion height P to the diameter of the target particle d. The support device facilitates the similarity of local geometry among different protrusions. In this way, the independent effect of protrusion height is ensured. It is worth mentioning that the local subsurface flow cannot maintain the similarity at different particle protrusion height. However, this variation is not considered as a vital factor because the present study focuses on the flow field above the bed roughness top.

Two-dimensional particle tracking velocimetry (PTV) was used to measure the velocity field in the streamwise-bed-normal plane along the flume centre line. The observation window was focused on the region in the vicinity of the target particle during the entrainment process. Tracing particles with a diameter of 10 μm were introduced to the water and illuminated by the light source, which includes a lightbox consisting of two boards and an LED light strip. A camera was located on the left side of the flume, at a distance of 1.5 m from the sidewall. The camera operated at a frame rate of 100 Hz. The captured images have a resolution of 1 400×14 00 pixels and are processed with streams to generate instantaneous flow field. The calculation grid of flow field has a temporal resolution of 0.01 s and a spatial resolution of 1 mm. In the present study, the measurement coordinate system adopted the right-hand rule. The x-, y- and z-axes are streamwise, transverse, and vertical directions. The origin of the coordinate system was at the centroid of the target particle located on the flume centreline, as shown in Fig. 1(a). The theoretical bed level was used to represent the hypothesised bed location for non-flat beds to take into account the effect of bed roughness. This value is set to be $0.20D$ beneath the top of the roughness elements, which follows Cameron[9], Dwivedi et al.[10], who deployed similar bed packing arrangements. Finely divided scales were attached to the flume sidewall for the measurement of water depth along the flume and to ensure flow uniformity. There were four rulers within the observation area three rulers at 0.5 m, 1.0 m and 1.5 m upstream of the target particle, and one ruler at 0.5 m downstream from the target particle.

Prior to the commencement of an experiment, the target particle was placed at a pre-determined location. Then the flow rate was increased slowly at a constant rate until the target particle's entrainment occurred. After each flow adjustment, the flow rate was kept constant for 10 s. Due to the consideration of flow stability, each flow measurement was conducted in 10 s prior to the particle entrainment. For each protrusion height, five entrainment experiments were conducted, resulting in 20 runs in total. The flow characteristics were the ensemble-average value of the five repeated experiments. For all experiments, a constant flow depth $H = 203$ mm was maintained along the flume throughout each test run to avoid the low relative submergence effect reported by Rouzes et al.[19]. The summary of the flow conditions for different particle protrusions is shown in Table 1. The fluid Reynolds number $(Re = u_{avg}H/\nu)$ and the Froude number were calculated based on the uniform flow depth and PTV-measured flow velocity, which were also calibrated using the corresponding cross-sectional average values. The results indicate that the flow is subcritical and fully turbulent for all the tested runs. In the present study, the status of entrainment is defined as when the particle is completely dislodged from its setting pocket. Slight vibrations of the target particle may occur prior to entrainment in some (but not all) experiments. As the main focus of this study is the "complete" entrainment, any particle vibration/ oscillation that did not induce a subsequent complete dislodgement is beyond the current scope and not further analysed and discussed.

2. Time-averaged flow characteristics

In this section, four flow parameters are investigated, including the time-averaged streamwise velocity $(\overline{u})$, time-averaged vertical velocity $(\overline{v})$, turbulent kinetic energy (TKE) and Reynolds shear stress $(\overline{\tau})$. TKE represents the turbulence level and

Table 1 Summary of test conditions

	Q /($m^3 \cdot s^{-1}$)	H /mm	d /mm	D /mm	P /mm	P/d	u_{avg} /($m \cdot s^{-1}$)	Re ($\times 10^3$)	Re_p	θ	Fr
Case 1	0.028	203	30	40	16.0	0.53	0.31	25.4	978	0.0028	0.34
Case 2	0.024	203	30	40	18.0	0.60	0.27	21.9	747	0.0160	0.30
Case 3	0.022	203	30	40	20.0	0.67	0.24	19.9	597	0.0100	0.27
Case 4	0.019	203	30	40	21.3	0.71	0.21	17.4	450	0.0060	0.24

Note: Q denotes flow rate, H is flow depth measured from $0.2D$ below the roughness elements, d is the diameter of the target particle, D is the diameter of the roughness spheres, P is the absolute protrusion height of the target particle measured from the roughness top, P/d is defined as the relative protrusion height, u_{avg} is the cross-sectional average velocity calculated from the flow rate, Re is flow Reynolds number, Re_p is particle Reynolds number, θ is Shields parameter and Fr is Froude number calculated based on H and u_{avg}.

reflects the energy extracted from the mean flow, as defined by Eq. (1). Reynolds shear stress potentially reflects the threshold entrainment condition and is defined by Eq. (2).

$$\mathrm{TKE} = \frac{1}{2}(\overline{u'^2} + \overline{v'^2}) \tag{1}$$

$$\overline{\tau} = -\rho\overline{u'v'} \tag{2}$$

where ρ is water density, u' and v' denote the instantaneous streamwise and vertical velocity fluctuation, respectively, and the overbar indicates a time-average quantity. Both the spatial distribution patterns and the vertical profiles of the abovementioned parameters are analysed. The former focuses on the parameter distribution along the flow direction and the latter is focused on the comparison of the vertical profiles between different protrusions. Papanicolaou et al.[20] classified the submergence of a particle H/D into high submergence $(H/D > 3.0)$, intermediate submergence $(1.0 < H/D < 3.0)$ and low submergence $(H/D < 1.0)$. According to this definition, the target particle belongs to the high submergence range, which means that bed roughness has an insignificant influence on the near-surface velocity. Thus, the flow velocity in the upper region is reasonably homogenous (e.g., $Z/D = 3.000 - 5.000$). As the main focal point of the present study is particle entrainment, the flow field in the near-bed region below $Z/D = 3.000$ (Z is the elevation from the theoretical bed level Z_0) is presented and discussed.

2.1 *Spatial distribution of the mean flow parameters*

Figure 3 demonstrates the distribution of time-averaged streamwise velocity $(\overline{u})$, time-averaged vertical velocity $(\overline{v})$, TKE and Reynolds shear stress $(\overline{\tau} = -\rho\overline{u'v'})$ in a vertical plane at the flume's centreline for all four particle protrusion heights. The figure is arranged as a matrix of subplots; that is, each line displays the distribution of one variable (e.g., $\overline{u}$) for different protrusion heights, and each row displays the distribution of different variables for the same protrusion height. The coordinate system is normalised by the roughness height D.

The first two rows of subplots in Fig. 3 show the spatial distribution of time-averaged streamwise $(\overline{u})$ and vertical velocity $(\overline{v})$, respectively. It can be seen that the protruded target particle provides a sheltered region (i.e., the recirculation zone) downstream of the particle, wherein the streamwise velocity is obviously reduced. Above $H/D = 1.5 - 2.0$, the vertical velocity becomes negative, indicating that downward flow is commonly distributed in the upper region. In contrast, positive time-averaged vertical velocities tend to occur near the target particle, and in particular, the maximum values are concentrated at the upper corner and sheltered area, which indicates the occurrence of flow separation and recirculation, respectively. Since the particle is highly protruding from the surrounding roughness particles, the approaching flow climbs over the surface of the target particle. Comparing the data for different protrusion heights shows that although the general distribution patterns of $\overline{u}$ and $\overline{v}$ are similar, the magnitudes of both variables reduce with increasing particle protrusion, provided that the bed arrangement regarding interaction with surrounding bed roughness elements is not altered.

The subplots in the third row of Fig. 3 show the spatial distribution of the time-averaged TKE. A uniform pattern is observed upstream of the target particle. However, the value of TKE is higher above and downstream of the target particle. The zone of enhanced TKE starts from the top half of the target

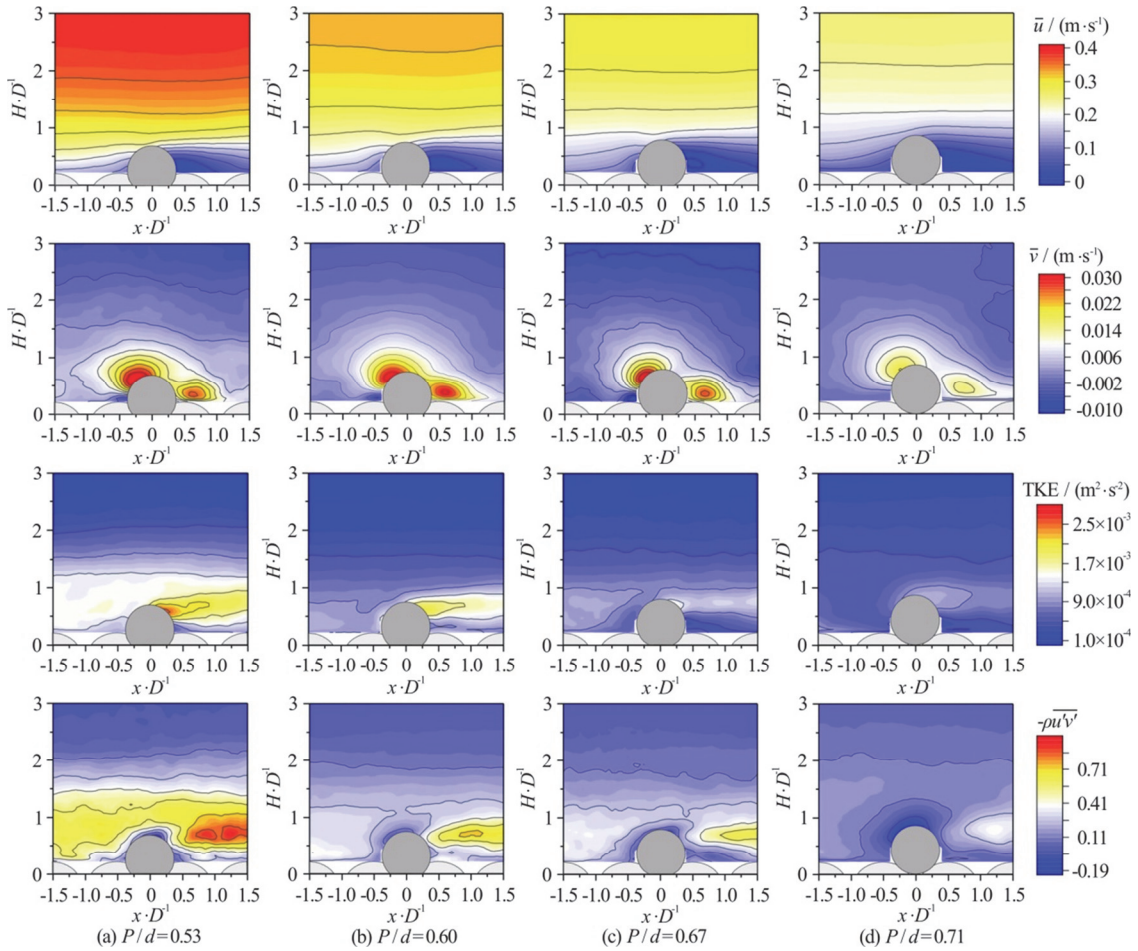

Fig. 3 (Color online) Spatial distributions of time-averaged streamwise velocity $(\bar{u})$, vertical velocity $(\bar{v})$, TKE and Reynolds shear stress $(\bar{\tau} = -\rho\overline{u'v'})$ for different particle protrusion heights. The plane is located at the flume's centreline. Flow direction from left to right

particle and extends further downstream for a distance of $1.25D$ approximately. This distance only varies slightly for different protrusion heights, but the intensity drops significantly with increasing protrusion. Taking $P/d = 0.53$ as an example, in the near-bed region, the mean value of the TKE is roughly 0.013 m^2/s^2 and the greatest value of TKE is 0.027 m^2/s^2, which is located at the downstream side of the particle's top. The TKE magnitude almost doubles due to the protrusion-induced turbulence (e.g., flow separation and recirculation). The observation of the high value of TKE downstream of the particle is generally consistent with the research of Lacey and Rennie[21], who used a cubic-shaped obstacle. As they suggested, the high value of TKE at the wake region of the obstructed object is related to the formation of the shear layer.

The fourth row of Fig. 3 shows the spatial distribution of the time-averaged Reynolds shear stress $\bar{\tau} = -\rho\overline{u'v'}$. The main finding in this figure is that negative Reynolds shear stress occurs above the target particle. According to Eq. (2), Reynolds shear stress is proportional to the value of $u'v'$. The occurrence of negative Reynolds shear stress indicates that the distribution of turbulent events around the target particle has changed, showing either ejection motions ($u' < 0$, $v' > 0$) or sweep motions ($u' > 0$, $v' < 0$). The variation of Reynolds shear stress is more directly related to both coarse-grained and fine-grained particles. This observation is discussed in detail in the later analysis of turbulent events around the particle regarding quadrant motion. Another finding is that the time-averaged Reynolds shear stress increases downstream of the target particle. The concentrated high Reynolds shear stress suggests the existence of a shear zone downstream of the particle, which is consistent with the observations of Lacey and Rennie[21], Lacey and Roy[22]. Taking $P/d = 0.53$ as an example, in the vertical direction, the shear zone exists between $H/D = 0.5$, 1.0 and is not attached to the bed; thus, the underlying roughness particles were sheltered. This result is consistent with the conclusion of Raus et al.[19] that the higher protrusion of the

coarse particle has less impact on the entrainment of underlying fine particles. Comparing all four protrusion heights shows that the negative stress zone around the target particle enlarges with increasing particle protrusion, and the general Reynolds stress magnitude also decreases in this process. More specifically, the positive Reynolds shear stress immediately downstream of the particle exhibits a more pronounced decrease with increasing particle protrusion than the general Reynolds shear stress.

Generally, the presence of the protruded particle disturbs the flow and turbulence distribution in the longitudinal direction. Therefore, seven locations were selected to analyse the vertical profiles of the flow parameters, i.e., $x/D = -1.5$, -1.0, -0.5, 0, 0.5, 1.0 and 1.5. The negative sign denotes upstream locations with respect to the target particle, and the positive sign represents downstream locations. Those profiles are analysed in the following sub-section.

2.2 *Vertical profiles of time-averaged flow characteristics*

For the flow over a rough bed, the time-averaged streamwise velocity profile follows the logarithmic law at a lower region of the flow depth, as defined by Eq. (3)

$$\frac{\overline{u}}{u_*} = \frac{1}{\kappa}\ln\left(\frac{Z}{k_s}\right) + Br \tag{3}$$

where $\overline{u}$ is the time-averaged velocity at vertical elevation Z, κ is the von Karman constant, taken as 0.4, u_* is shear velocity, which can be defined from a fitted logarithmic function, k_s is the roughness height, taken as D in the present paper and Br is the constant of integration. The profiles of the time-averaged streamwise velocity at selected locations are presented in Fig. 4. The time-averaged streamwise velocity profiles show a similar pattern at different particle protrusions. For each protrusion height, the profiles of the time-averaged streamwise velocity at different longitudinal locations collapse well above $Z/D = 1.0$.

The logarithmic function (Eq. (3)) is used to fit the velocity above $Z/D = 1.000$, as shown by the red dashed line in Fig. 4. The velocity in the range of $1.000 < Z/D < 3.000$ fits well with the logarithmic law. The values of u_* and Br were found through the bi-square method. For four different protrusion heights ($P/d = 0.53$, 0.60, 0.67 and 0.71), the values of u_* are 0.040 m/s, 0.032 m/s, 0.030 m/s and 0.028 m/s, respectively; the values of Br are 7.25, 7.80, 8.20 and 6.40, respectively. The value of R^2 is around 0.98 for each protrusion case, indicating a reasonable fitting result. Below $Z/D = 1.000$, the velocity profile deviates from the fitted logarithmic distribution at the near-particle region because of the

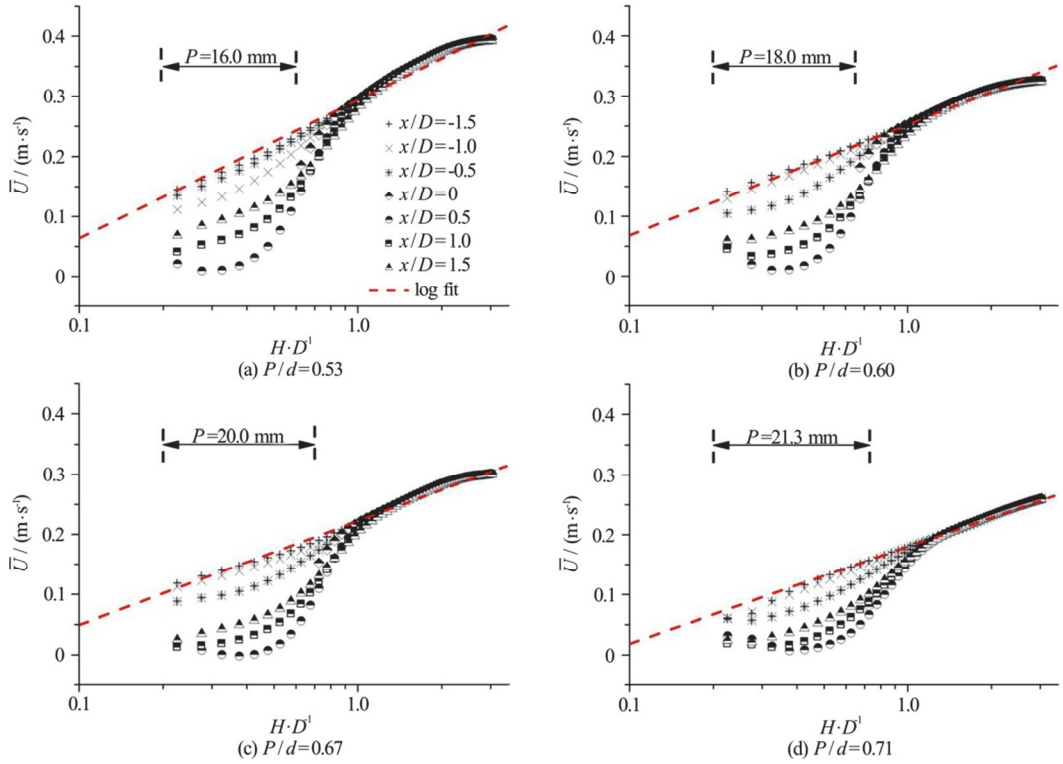

Fig. 4 (Color online) Vertical profile of time-averaged streamwise velocity at different locations along the flow direction. X-axis is in logarithmic scale

influence of particle protrusion. With further distance downstream from the particle ($x/D=1.5$), the impact of the particle protrusion becomes weak, and the velocity starts recovering to the logarithmic distribution. According to the research of Dey et al.[23], the recovery distance of the time-averaged velocity was roughly $8d$, which is much larger than the value in the present study. It is obvious that the velocity has not been completely recovered at $x=1.5D$ (Fig. 4). The limited observation window in the present study (with $3.0D$ width in a streamwise direction) makes it hard to decide the exact recovery distance of velocity, thus further investigation might be required. Since the present study is focused on the near-particle flow field, the discovery distance of the velocity is not considered here. Besides, the velocity profiles at $x/D=-1.5$, -1.0 are quite comparable. This similarity reflects that the approach flow upstream of $x/D=1.0$ is steady and uniform for all the tested protrusion cases. It should also be noted that in Fig. 5, the flow velocity will not necessarily reduce to zero over the top of bed roughness particles (i.e., $Z/D=0.200$), to which the velocity measurement is truncated. Although it is usually assumed that the fluid velocity is zero/or approaching to zero at the solid boundary which is flat and non-slip, this rule seems not to be preserved if we consider the existence of a rough surface (see Fig. 4). A possible explanation is that a series of cavity flows occur between different roughness particles, which complicates the velocity distribution at the surface along the centreline. This complication might be enhanced with coarser target and roughness particles. This phenomenon underpins the selection of $0.2D$ beneath the roughness top as the theoretical bed level.

In Fig. 5, the time-averaged vertical velocity profiles show negative values in the upper region of flow depth (approximately $Z/D>2.000$) but gradually increase to be positive towards the bed. The boundary between the upper and lower flow regions varies for different particle protrusions and horizontal locations without a clear trend. Comparatively, positive vertical velocity tends to be more predominant when close to and immediately above the target particle. The existence of positive time-averaged vertical velocity is different from the findings of Cameron[9], Dwivedi et al.[10], who used similar experimental setups but only observed negative vertical velocities. The main reason is that those studies used relatively small protrusion heights of the target particle ($P/d\leq 0.26$). Therefore, it is reasonable to conclude that the presence of a highly protruding particle changes the adjacent flow pattern more significantly than deeply embedded particles, especially in terms of vertical fluid motion. In the near-particle region ($x/D=-0.5$, 0, 0.5), the time-averaged vertical velocity reaches a maximum value at the particle's top. However, with a higher protrusion height, the required vertical velocity

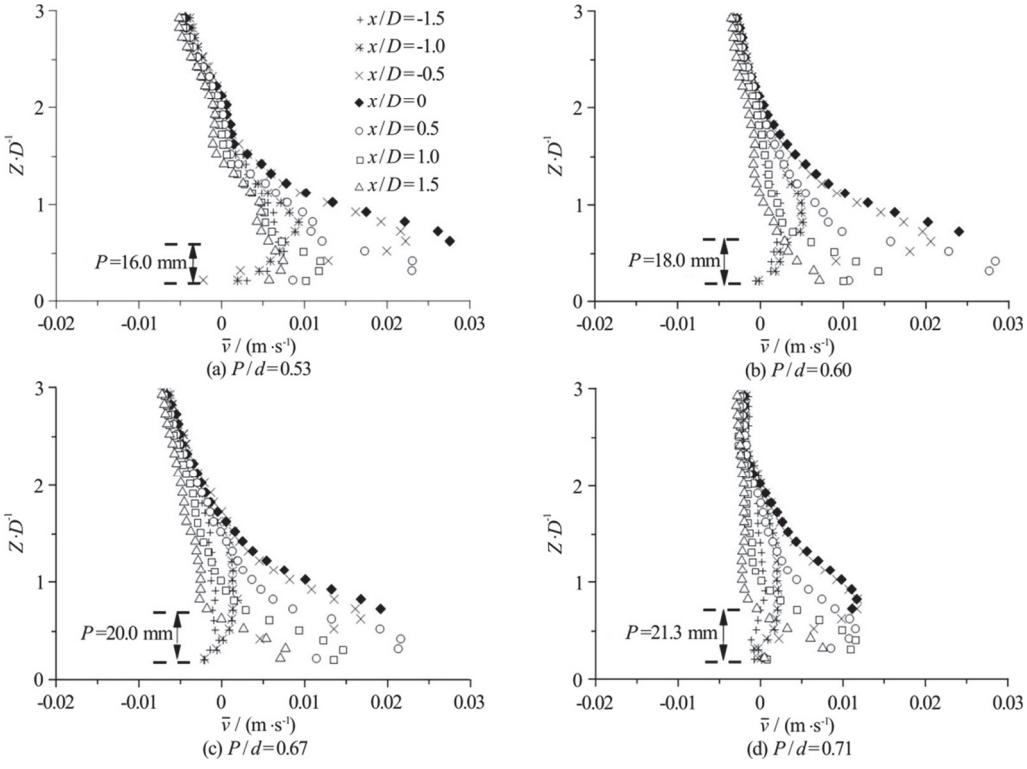

Fig. 5 Vertical profile of time-averaged vertical velocity at different locations along the flow direction

component at the moment of entrainment reduces, indicating a less threshold for particle motion due to the reduced embedment. This reduction is in accordance with the reduction of the approaching flow strength at entrainment.

As mentioned previously, the spatial distribution of time-averaged flow parameters is homogenous in the upper region of flow depth. This characteristic is also seen in the TKE distribution, where the influence of longitudinal location and protrusion height diminishes for $Z/D>2.000$ approximately. In Fig. 6, the vertical profile of the TKE at different longitudinal locations generally follows a similar pattern. The peak TKE value is located close to the particle top. Comparing the TKE distribution for different protrusion heights shows that, from $P/d=0.53$ to $P/d=0.71$, the maximum TKE value decreases from 0.22×10^{-2} m^2/s^2 to 0.1×10^{-2} m^2/s^2, which is similar to the trends of flow velocities. This result indicates that the particle entrainment with a lower protrusion requires more turbulence energy and momentum to be transferred to the exposed particle. In general, although the near-bed TKE magnitude is enhanced due to the particle protrusion and the corresponding turbulence field, its maximum value is also highly related to the mean approaching flow velocity at the moment of entrainment.

The vertical distribution of the time-averaged Reynolds shear stress is shown in Fig. 7. Except at the particle's centre $(x/D=0)$, the vertical distribution pattern of the time-averaged Reynolds shear stress is similar to the trends of TKE. The extrapolation of Reynolds shear stress distribution is widely used to obtain the bed shear stress and is further used as an indicator for the threshold entrainment condition. Following this method, the threshold shear stress was derived from the linear extension of the profiles in the upper region to the theoretical bed (red dashed lines in Fig. 7). Approximately, the threshold bed shear stress was 0.90 N/m^2, 0.55 N/m^2, 0.45 N/m^2 and 0.30 N/m^2 for $P/d=0.53$, 0.60, 0.67 and 0.71, respectively. The threshold shear stress decreases as the protrusion height increases, as expected from previous research[5, 8] and also aligns with the analysis of previous variables in this study. However, it is found in Fig. 6 that Reynolds shear stress just above the top of the particle may turn either positive or negative and does not show a clear relationship with the protrusion heights (increases from Figs. 7(a) to 7(d)) or approach flow strength (decreases from Figs. 7(a) to 7(d)). In Fig. 7(d), Reynolds shear stress at $x/D=0$ starts becoming negative at a relatively long distance above the particle, which is significantly different from other cases. This phenomenon indicates that Reynolds shear stress might not be the predominant factor determining the initial movement of a highly protruding particle. As Reynolds shear stress is used to represent turbulent fluctuations in fluid momentum, the results in Fig. 7 indicate that the turbulent events at the particle top behave anomalously due to the flow

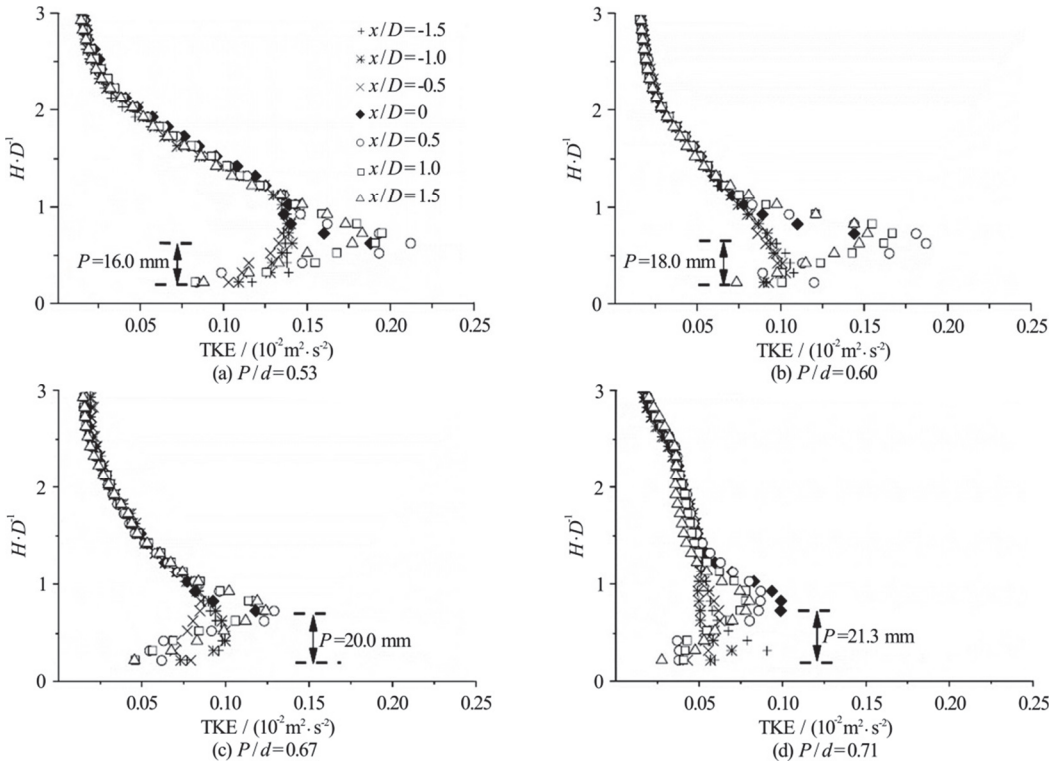

Fig. 6 Vertical profile of time-averaged TKE at different locations along the flow direction

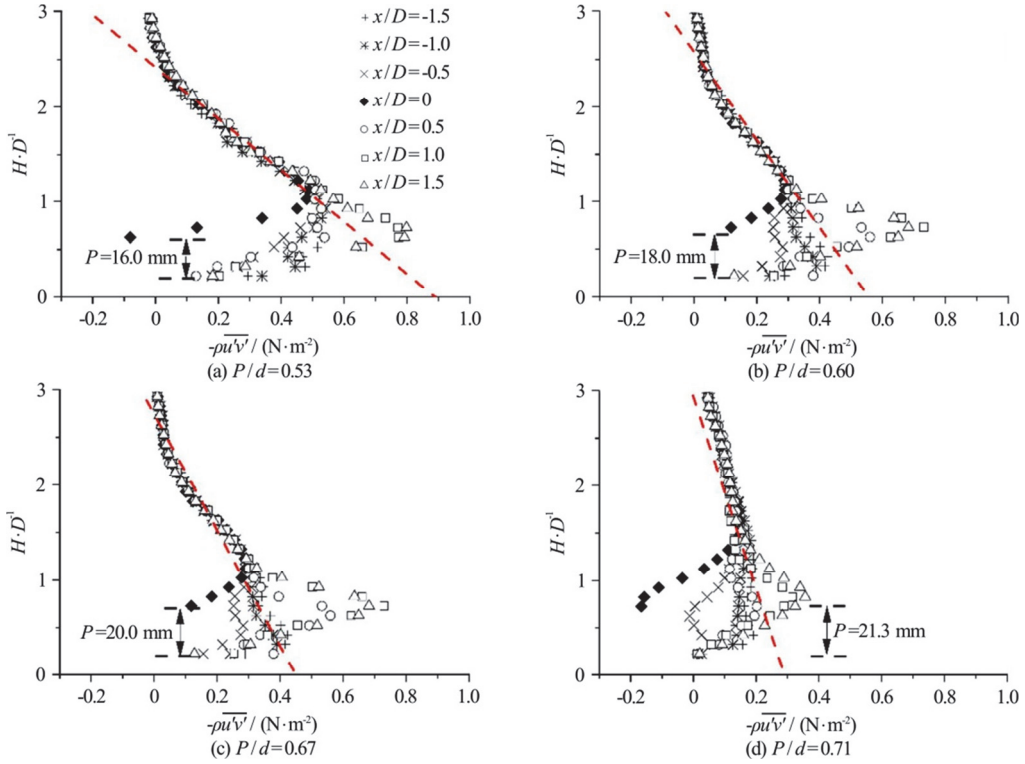

Fig. 7 (Color online) Vertical profile of time-averaged Reynolds shear stress along the flow direction

separation and the corresponding flow field variation. More analysis in terms of those turbulent behaviours is needed.

In summary, the protrusion of a coarse particle results in a substantial disturbance to the nearby flow field, but the extent of disturbance at the moment of entrainment is also dependent on the general flow strength, e.g., mean approaching flow velocity. Due to the presence of a protruded particle, strong turbulent events occur at the near region of the particle. Although it is obvious that threshold Reynolds shear stress decreases above and towards the particle, the lack of a clear relationship with particle protrusion suggests a more complex mechanism of particle entrainment. Therefore, the analysis of particle entrainment and the corresponding flow condition requires information on both general flow strength and microscopic structures.

3. Turbulent events around the protruding particle

Further analysis of the near-particle turbulent events is conducted during the time before the instant of entrainment and focuses on the flow quadrant motions. The vertical location closest to the particle top is selected for the analysis of turbulent events. This location was chosen because strong turbulence was observed here (Fig. 6). Specifically, the vertical locations are $Z/D=0.625$, 0.675, 0.725 and 0.775 for $P/d=0.53$, 0.60, 0.67 and 0.71, respectively.

As described in the introduction, the velocity fluctuation in the streamwise direction u' and in vertical direction v' can be classified into four quadrants: outward interactions (Q1), ejections (Q2), inward interactions (Q3) and sweeps (Q4). In this section, the results of quadrant analysis at the same seven locations as used for the profiles are presented. Two parameters were usually used to characterise the quadrant events: the fraction of the shear stress in the ith quadrant, $S^F_{i,\dot{H}}$, and the duration factor of the ith quadrant, $T^F_{i,\dot{H}}$. The former indicates the relative contribution of the turbulent events to the Reynolds shear stress, and the latter is used to assess the predominant quadrant during a specific time. The following equations define these parameters:

$$T^f_{i,H}=\frac{1}{N}\sum_{i=1}^{N} I_{i,\dot{H}}(u',w') \tag{4}$$

$$S^f_{i,\dot{H}}=\frac{1}{N\overline{u'w'}}\sum_{i=1}^{N} I_{i,\dot{H}}(u',w') \tag{5}$$

where $i=1,2,3,4$ represents the quadrant number, N is the total number of the velocity data during the study period, u' and w' denote the temporal fluctuation of streamwise and vertical velocity, respectively. The variable $I_{i,\dot{H}}$ on the right-hand side of Eqs. (4), (5) is a function that can expressed as:

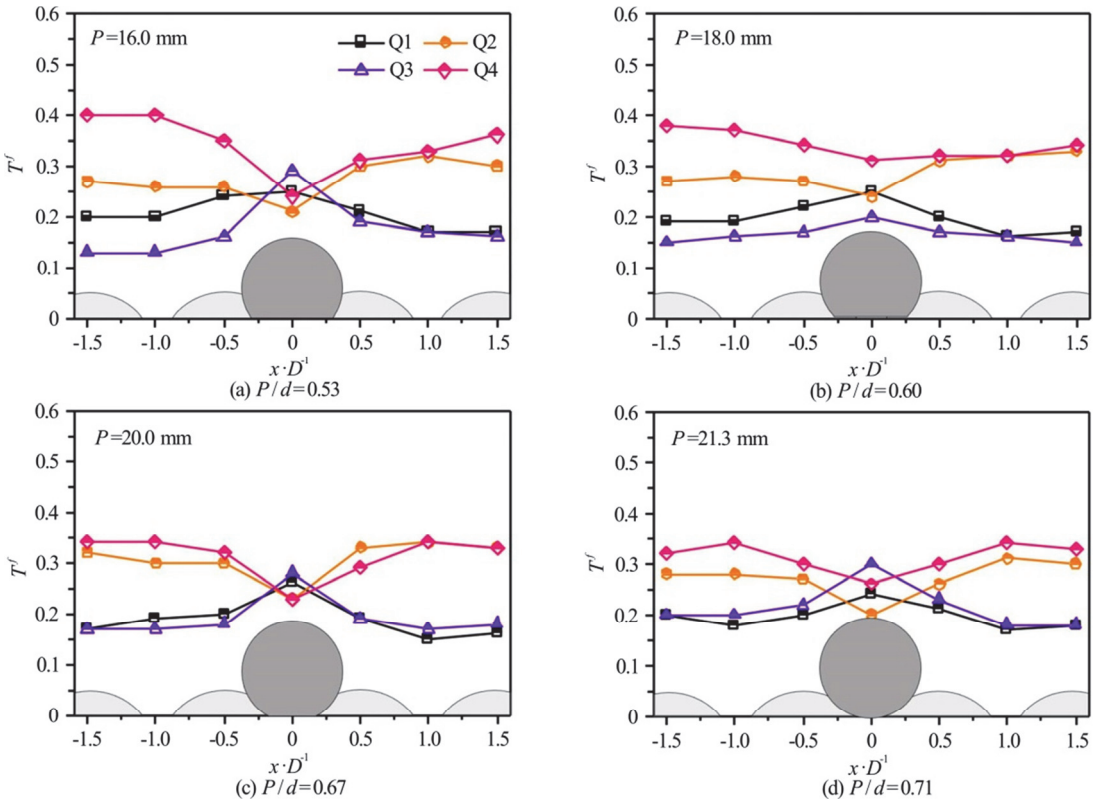

Fig. 8 (Color online) Duration factor in longitudinal direction of top particle region

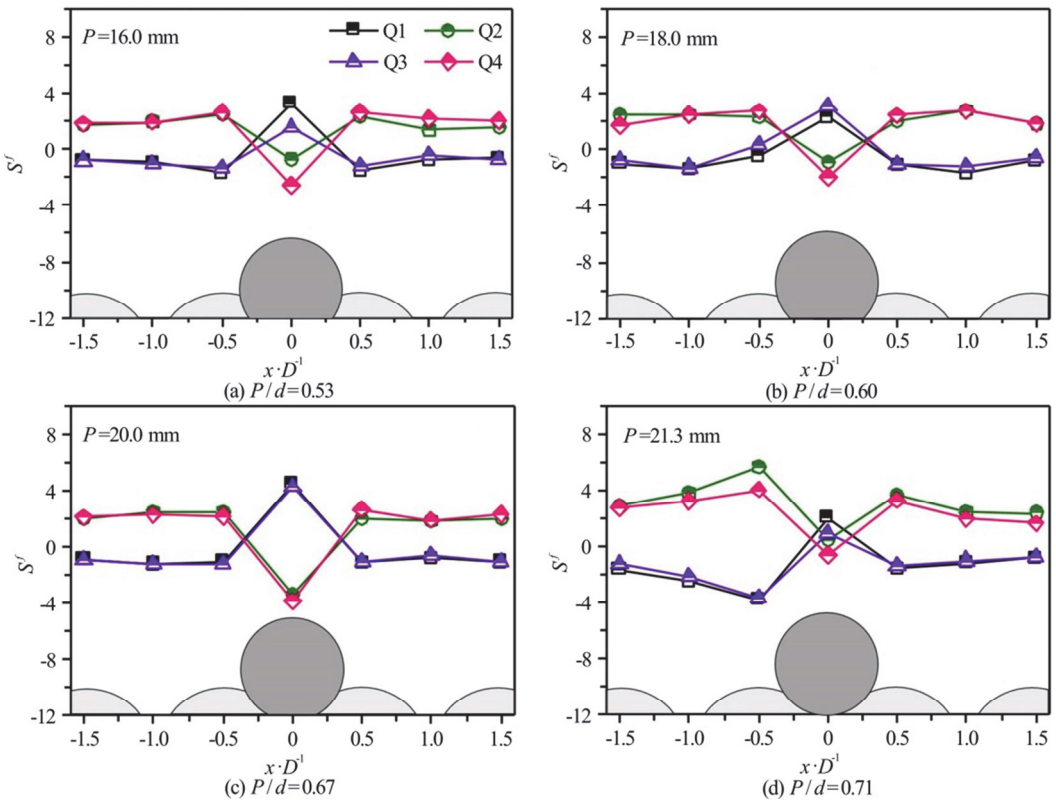

Fig. 9 (Color online) Shear stress faction at the particle top

$$I_{i,\dot{H}}(u',w')=1 \quad \text{if} \quad |u'w'| \geq \dot{H}u'_{\text{rms}}v'_{\text{rms}} \tag{6a}$$

$$I_{i,\dot{H}}(u',w')=0 \quad \text{otherwise} \tag{6b}$$

where u'_{rms} and v'_{rms} are the root mean square (rms) values of the streamwise and vertical velocity fluctuations, respectively. $\dot{H}$ is termed the hole size, which can be used to eliminate insignificant velocity fluctuations. The value of hole size $\dot{H}$ varied in different studies[16, 18, 23]. Here, for the aim of comparison with previous entrainment experiments with similar setups[9-10], $\dot{H}=0$ was applied. Generally, the function $I_{i,\dot{H}}$ is used to trigger cumulative measurements based on the judgement of the turbulence fluctuation at each moment in a specific duration. The duration factor and fractional shear stress are presented in Figs. 8, 9, respectively.

From Fig. 8, the longitudinal distribution of the duration factors at different particle protrusion heights is shown. At the upstream locations $(-1.5 < x/D < -0.5)$ and downstream locations $(0.5 < x/D < 1.5)$, the sweep turbulent events (Q2) and ejection events (Q4) are predominant (comprising approximately 60-70 percentage of the total turbulent events). More specifically, sweep events are predominant upstream of the target particle, while ejections and sweep events are comparable downstream of the particle. This result is consistent with findings from previous studies in which the turbulent events around large spherical roughness were investigated[18, 23]. At the upstream particle region, the occurrence of sweep events is less frequent as particle protrusion increases, whereas the relative duration of inward interactions slightly increases with increasing particle protrusion. In contrast, in the downstream region, the relative duration of each turbulent event remains similar for different particle protrusions. The occurrence of each turbulent event seems to be comparable and shows no specific trend between different particle protrusions at $x/D=0$. Nelson et al.[15], Papanicolaou et al.[24] showed that ejections and sweep events have a high probability of occurrence in the flow over a uniformly sized rough bed, which is observed at upstream and downstream locations. This result suggests that the approaching turbulent flow is well developed. However, at the near particle region, the protruding particle causes the redistribution of turbulent events. While approaching the particle top, the outward interaction (Q1) and inward interaction (Q3) become predominant, and the ejection (Q2) and sweep (Q4) events have less occurrence compared to Q1 and Q3. This phenomenon can be clearly seen at the particle top $(x/D=0)$.

In Fig. 9, the shear stress fraction of each quadrant is comparable at both downstream and upstream regions for different particle protrusions. Although ejection events are less frequent than sweep events, the relative contribution of these two events to the Reynolds shear stress is roughly the same. Upstream and downstream of the target particle, the sweep and ejection events positively contribute to the Reynolds shear stress, and the outward and inward interactions negatively contribute to Reynolds shear stress. In contrast, the contribution of each quadrant event to the shear stress are reversed near the particle. This finding is because the averaged Reynolds shear stress is negative at the particle top. It is also observed that the positive and negative fractions tend to negate each other at the particle top, which explains the low Reynolds shear stress at this location. These results reveal that the particle protrusion leads to a variation of turbulent event distribution at the near particle region. If the quadrant analysis was conducted at a single location, the role of turbulent events on the particle entrainment might be misunderstood. Thus, caution needs to be exercised when linking local quadrant events to particle entrainment.

Nelson et al.[15] found that the flow velocity measured approximately 0.1 s before particle entrainment is highly correlated with the particle entrainment. On that basis, the velocity measurement during the 0.1 s before entrainment in this study is used to identify the representative turbulent event. For this analysis, the data of repeated experiments were combined to ensure the reliability of statistics. Figure 10 presents the relative occurrence of turbulent events associated with particle entrainment along the longitudinal direction.

As shown in Fig. 10, inwards interactions and ejections rarely occurred at upstream locations compared to outward interactions and sweep events. The occurrence of sweep events decreases at the near-particle region, whereas the occurrence of outward interactions increases at this region. The main finding here is that the outward interaction events, which are less frequent on average (roughly 20% of the total events, see Fig. 8), have a higher occurrence during particle entrainment. In contrast to the present result, Cameron[9], Dwivedi et al.[10, 25] found that outward interactions were less frequent compared to sweep events in their entrainment experiments. Sweep events feature high-speed fluid being directed downwards towards the target particle, resulting in "Bernoulli" lift compared with outward interactions. The particle protrusion has a range of $[0, 0.25]$ in the experiments of Cameron[9], Dwivedi et al.[10, 25], which is much lower than the values in present study. While the target particle highly protrudes over surrounding particles in the present study, the

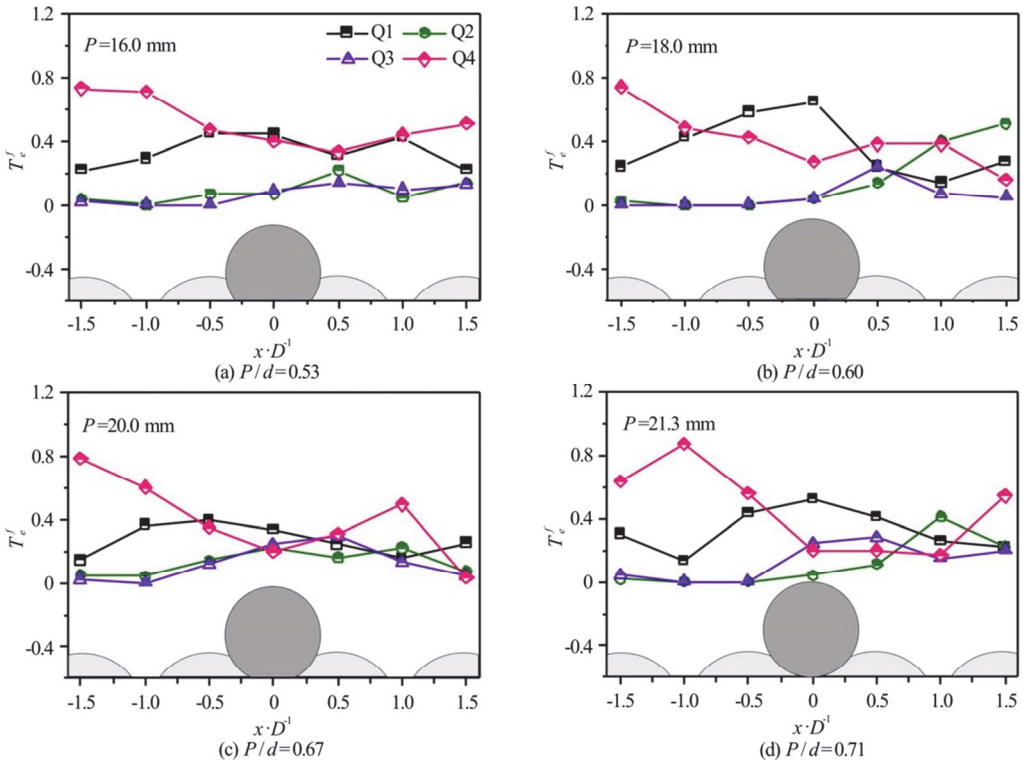

Fig. 10 (Color online) Relative occurrence of entrainment events at the particle top

approaching flow tends to climb over the obstruction (Fig. 3) and cause vertical acceleration of fluid. As a result, it can be expected that the outward interaction event occurs more frequently than in the cases with less protrusion heights. The outward interactions correspond to the negative Reynolds shear stress. Near the target particle, the predominance of outward interactions during particle entrainment indicates that the low Reynolds shear stress may not be entirely responsible for particle dislodgement. However, Cecchetto et al.[16] noted that outward interactions were also important for particle dislodgement, especially when other moving particles are around the target particle. They also mentioned that the Bernoulli principle does not entirely explain the vertical forces. Outward interaction events associated with upward vertical velocities also provide drag-based vertical forces[9]. Overall, outward interactions and sweep events have positive streamwise velocity fluctuation, corresponding to the strong drag force exerted on the target particle[26-27]. Thus, the drag-based mechanism, different from the Reynolds shear stress associated with the strong velocity gradient, may contribute significantly to particle entrainment under the present experimental conditions. This result also suggests that the threshold Reynolds shear stress may not accurately predict the entrainment condition of a highly protruding particle.

4. Conclusions

The disturbance to the flow field caused by an exposed coarse particle is crucial for analysing the particle's entrainment condition. The experimental results in this study show that the particle protrusion leads to a substantial change of the nearby flow characteristics; in turn, the change of the near-bed flow characteristics influences the entrainment of the protruded coarse particle. The main findings are summarised as follows:

(1) Within the tested protrusion range ($0.53 < P/d < 0.71$), the distribution of flow characteristics exhibits a considerable degree of similarity between different protrusion heights. However, the magnitude of flow parameters at entrainment is dependent on the approach flow strength at that instant, which is inversely proportional to the protrusion height.

(2) At the near-particle and downstream locations, the vertical profiles of time-averaged streamwise velocity deviated from the logarithmic law due to the protrusion of the target particle. Upward flows are generally observed in the near-bed region, with peak time-averaged vertical velocity occurring above the protruded particle.

(3) TKE values are high above the protruded particle, which is consistent with the presence of the

protruded particle leading to strong momentum transfer. A separated shear zone forms downstream of the target particle.

(4) Low Reynolds shear stress was observed above the protruded particle for all the tested protrusion heights. Counter turbulent events (i.e., outwards interactions and inward interactions, and sweeps and ejections) tended to annul each other at the near particle region, leading to a reduction of Reynolds shear stress.

(5) The turbulent events associated with entrainment showed the prevalence of outward interactions (Q1) and sweep events (Q4). This finding indicates that the drag force associated with strong longitudinal velocity may play an important role in the initial dislodgement of protruded particles. It further suggests that shear stress may not accurately predict the threshold entrainment condition.

It should be noted that a simplified regular bed arrangement was used in this study to enhance understanding of the effect of particle protrusion on the nearby flow field. More investigation using naturally distributed sediment particles under laboratory situations is recommended. Despite the qualitative nature of the current findings, the general trend of entrainment mechanism for different protrusion heights is discovered, which facilitates the further derivation of quantitative formulas when wider parameter ranges become available. Another limitation of this study is that the lateral flow structure still remains unknown. With the existing experimental setup, the particle entrainment primarily follows the longitudinal and vertical direction. Such particle movement process indicates that the two-dimensional PTV is appropriate for the current situations. However, three-dimensional flow structures should be examined for more complex scenarios in which entrainment requires significant lateral movement, e.g., with different alignments of downstream particles.

Acknowledgement

The first author would like to thank the financial support of the Chinese Scholar Council (CSC) and The University of Auckland.

Compliance with Ethical Standards

Conflict of interest: The authors declare that they have no conflict of interest.

Ethical approval: This article does not contain any studies with human participants or animals performed by any of the authors.

References

[1] Yager E. M., Kirchner J. W., Dietrich W. E. Calculating bed load transport in steep boulder bed channels [J]. *Water Resources Research*, 2007, 43(7): W07418.

[2] Grams P. E., Wilcock P. R. Equilibrium entrainment of fine sediment over a coarse immobile bed [J]. *Water Resources Research*, 2007, 43(10): W10420.

[3] Raus D., Moulin F. Y., Eiff O. The impact of Coarse-Grain protrusion on near-bed hydrodynamics [J]. *Journal of Geophysical Research: Earth Surface*, 2019, 124(7): 1854-1877.

[4] Wiberg P. L., Smith J. D. Velocity distribution and bed roughness in high‐gradient streams [J]. *Water Resources Research*, 1991, 27(5): 825-838.

[5] Fenton J. D., Abbott J. E. Initial movement of grains on a stream bed: The effect of relative protrusion [J]. *Proceedings of the Royal Society of London*, 1977, 352(1671): 523-537.

[6] Vollmer S., Kleinhans M. G. Predicting incipient motion, including the effect of turbulent pressure fluctuations in the bed [J]. *Water Resources Research*, 2007, 43(5): W05410.

[7] Chin C. O. Stream bed armouring [D]. Doctoral Thesis, Auckland, New Zealand: The University of Auckland, 1985.

[8] Coleman S. E., Melville B. W., Gore L. Fluvial entrainment of protruding fractured rock [J]. *Journal of Hydraulic Engineering, ASCE*, 2003, 129(11): 872-884.

[9] Cameron S. M. Near-boundary flow structure and particle entrainment [D]. Doctoral thesis, Auckland, New Zealand: The University of Auckland, 2006.

[10] Dwivedi A., Melville B. W., Shamseldin A. Y. et al. Flow structures and hydrodynamic force during sediment entrainment [J]. *Water Resources Research*, 2011, 47(1): W01509.

[11] Drake T. G., Shreve R. L., Dietrich W. E. et al. Bedload transport of fine gravel observed by motion-picture photography [J]. *Journal of Fluid Mechanics*, 1988, 192: 193-217.

[12] Booij R., Hofland B. Measurement of the mechanisms of stone entrainment [J]. *Proceedings 2nd International Conference on Scour and Erosion (ICSE-2)*, Singapore, 2004.

[13] Schobesberger J., Lichtneger P., Hauer C. et al. Three-dimensional coherent flow structures during incipient particle motion [J]. *Journal of Hydraulic Engineering, ASCE*, 2020, 146(5): 04020027.

[14] Thorne P. D., Williams J. J., Heathershaw A. D. In situ acoustic measurements of marine gravel threshold and transport [J]. *Sedimentology*, 1989, 36(1): 61-74.

[15] Nelson J. M., Nelson J. M., Shreve R. L. et al. Role of near-bed turbulence structure in bed load transport [J]. *Water Resources Research*, 1995, 31(8): 2071-2086.

[16] Cecchetto M., Tregnaghi M., Bottacin-Busolin A. et al. Statistical description on the role of turbulence and grain interference on particle entrainment from gravel beds [J]. *Journal of Hydraulic Engineering, ASCE*, 2017, 143(1): 1-9.

[17] Wu F. C., Shih W. R. Entrainment of sediment particles by retrograde vortices: Test of hypothesis using near-particle observations [J]. *Journal of Geophysical Research: Earth Surface*, 2012, 117(3): F03018.

[18] Golpira A., Baki A. B. M., Zhu D. Z. Turbulent events around an intermediately submerged boulder under wake interference flow regime [J]. *Journal of Hydraulic Engineering, ASCE*, 2021, 147(7): 06021005.

[19] Rouzes M., Moulin F. Y., Florens E. et al. Low relative-submergence effects in a rough-bed open-channel flow [J]. *Journal of Hydraulic Research*, 2019, *57*(2): 139-166.

[20] Papanicolaou A. N., Tsakiris A. G., Wyssmann M. A. et al. Boulder array effects on bedload pulses and depositional patches [J]. *Journal of Geophysical Research: Earth Surface*, 2018, 123(11): 2925-2953.

[21] Lacey R. W. J., Rennie C. D. Laboratory investigation of turbulent flow structure around a bed-mounted cube at multiple flow stages [J]. *Journal of Hydraulic Engineering, ASCE*, 2012, 138(1): 71-84.

[22] Lacey R. W. J., Roy A. G. The spatial characterization of turbulence around large roughness elements in a gravel-bed river [J]. *Geomorphology*, 2008, 102(3-4): 542-553.

[23] Dey S., Sarkar S., Bose S. K. et al. Wall-wake flows downstream of a sphere placed on a plane rough wall [J]. *Journal of Hydraulic Engineering, ASCE*, 2011, 137(10): 1173-1189.

[24] Papanicolaou A. N., Diplas P., Dancey C. L. et al. Surface roughness effects in near-bed turbulence: Implications to sediment entrainment [J]. *Journal of Engineering Mechanics*, 2001, 127(3): 211-218.

[25] Dwivedi A., Melville B., Raudkivi A. J. et al. Role of turbulence and particle exposure on entrainment of large spherical particles in flows with low relative submergence [J]. *Journal of Hydraulic Engineering, ASCE*, 2012, 138(12): 1022-1030.

[26] Schmeeckle M. W., Nelson J. M., Shreve R. L. Forces on stationary particles in near-bed turbulent flows [J]. *Journal of Geophysical Research: Earth Surface*, 2007, 112(2): F02003.

[27] Marion A., Tregnaghi M. A new theoretical framework to model incipient motion of sediment grains and implications for the use of modern experimental techniques (Experimental and computational solutions of hydraulic problems) [M]. Berlin, Heidelberg, Germany: Springer, 2013, 85-100.